Multiwavelength AGN Surveys and Studies
Proceedings IAU Symposium No. 304, 2013
A. M. Mickaelian & D. B. Sanders, eds.

doi:10.1017/S1743921314003822

Identifying Distant AGNs

Laura Trouille[1,2], Amy Barger[3,4] and Christy Tremonti[3]

[1]Dept. of Physics and Astronomy & Center for Interdisciplinary Exploration and Research in Astrophysics (CIERA), Northwestern University, Evanston, IL, USA
email: l-trouille@northwestern.edu

[2]Dept. of Astronomy, The Adler Planetarium, Chicago, IL, USA
email: barger@astro.wisc.edu, tremonti@astro.wisc.edu

[3]Dept. of Astronomy, University of Wisconsin – Madison, Madison, WI, USA
email: barger@astro.wisc.edu, tremonti@astro.wisc.edu

[4]Institute for Astronomy, University of Hawaii, Honolulu, HI, USA
email: barger@astro.wisc.edu

Abstract. The Baldwin, Phillips, and Terlevich emission-line ratio diagnostic ([OIII]/Hβ versus [NII]/Hα, hereafter BPT diagram) efficiently separates galaxies whose signal is dominated by star formation (BPT-SF) from those dominated by AGN activity (BPT-AGN). Yet the BPT diagram is limited to $z < 0.5$, the redshift at which [NII]λ6584 leaves the optical spectral window. Using the Sloan Digital Sky Survey (SDSS), we construct a new diagnostic, or TBT diagram, that is based on rest-frame $g - z$ color, [NeIII]λ3869, and [OII]$\lambda\lambda$3726 + 3729 and can be used for galaxies out to $z < 1.4$. The TBT diagram identifies 98.7% of the SDSS BPT-AGN as TBT-AGN and 97% of the SDSS BPT-SF as TBT-SF. Furthermore, it identifies 97% of the OPTX *Chandra* X-ray selected AGNs as TBT-AGN. This is in contrast to the BPT diagram, which misidentifies 20% of X-ray selected AGNs as BPT-SF.

Keywords. cosmology: observations — galaxies: active — galaxies: nuclei — galaxies: Seyfert — galaxies: distances and redshifts — X-rays: galaxies

1. Introduction

The most commonly used optical emission-line diagnostic for separating star-forming galaxies from type II Active Galatic Nuclei (AGNs) relies on [OIII]λ5007/Hβ versus [NII] λ6584/Hα (Baldwin *et al.* 1981; Veilleux *et al.* 1987), hereafter referred to as the BPT diagram. The basic idea is that the emission lines in star-forming galaxies are powered by massive stars, so there is a well-defined upper limit on the intensities of the collisionally excited lines relative to the recombination lines (such as Hα or Hβ). In contrast, AGNs are powered by a source of far more energetic photons, making the collisionally excited lines more intense relative to the recombination lines. Two demarcations are commonly used for identifying AGN-dominated galaxies versus star formation dominated galaxies – (1) the Kewley *et al.* (2001) theoretical division between galaxies whose extreme ultraviolet (EUV) ionizing radiation field is dominated by an AGN ($> 50\%$) and those dominated by star formation and (2) the Kauffmann *et al.* (2003) empirical demarcation based on the location of the Sloan Digital Sky Survey (SDSS) star-forming galaxies. Galaxies that lie between these two curves are often referred to as composite galaxies. Hereafter, we refer to these categories as BPT-AGN, BPT-SF, and BPT-comp.

The BPT diagram is limited in its use with optical spectra to galaxies with $z < 0.5$ (the redshift at which [NII] leaves the optical spectral window). A number of groups have extended optical emission line diagnostics to higher redshifts by only using lines at

the blue end of the spectrum. Lamareille (2010) replaced [NII]/Hα with [OII]λ3726 + λ3729/Hβ, creating the 'blue diagram', which can be used to classify galaxies out to $z < 0.9$. Yan *et al.* (2011) and Juneau *et al.* (2011) introduced the CEx and MEx diagnostics, respectively, in which they replaced [NII]/Hα with rest-frame $U - B$ color (CEx) or with stellar mass (MEx). Because these diagnostics rely on Hβ at λ4861 Å, their use with optical spectra is limited to $z < 1$.

At higher redshifts the Stasinska *et al.* (2006) DEW diagnostic, based on $D_n[4000]$, [NeIII]λ3869, and [OII], can be used with optical spectra out to $z < 1.4$, at which point the lines move into the infrared. [NeIII] emission indicates the presence of highly ionized gas and is much stronger than [OII] in high-excitation AGNs. However, because $D_n[4000]$ requires a sufficiently high signal-to-noise continuum and requires the survey to be spectrophotometrically calibrated, its usage with distant galaxies is limited.

In Trouille *et al.* (2011) we examined whether rest-frame $g - z$ color, which requires near-infrared imaging at the higher redshifts, is a compelling replacement for $D_n[4000]$. We referred to this new diagnostic as the TBT diagram.

2. Results

2.1. *Optical and X-ray Samples*

To construct our optically selected sample of galaxies, we used the SDSS spectroscopic data from Data Release 8 (DR8). Our SDSS BPT sample consists of the 243,865 SDSS galaxies that have Hα, [NII], Hβ, and [OIII] fluxes with signal-to-noise ratio (SNR) greater than five (out of the 818,333 unique galaxy spectra in the DR8 sample). Of these SDSS BPT galaxies, 23,048 also have both [NeIII] and [OII] fluxes with SNR > 5. We refer to these as our SDSS TBT sample.

Our OPTX X-ray selected sample consists of 1789 X-ray sources from the *Chandra* Deep Field North (CDFN; Alexander *et al.* 2003), the *Chandra* Large Area Synoptic X-ray Survey (CLASXS; Yang *et al.* 2003), and the *Chandra* Lockman Area North Survey (CLANS; Trouille *et al.* 2008; Trouille *et al.* 2009; Wilkes *et al.* 2009). We have spectroscopically observed 84% of the OPTX sources (for details of the observations and reduction process, see Trouille *et al.* 2008). We limited our study to the 561 OPTX X-ray sources with spectroscopic redshifts, whose $2-8$ keV flux has a significance greater than 3 σ, and whose $L_X > 10^{42}$ erg s^{-1}.

2.2. *TBT Diagnostic*

In Figure 1 we plot our TBT diagnostic – $^{0.0}(g - z)$ color versus log([NeIII]/[OII]) – for our SDSS TBT sample. The top, middle, and bottom panels show the locations of the BPT-AGN, BPT-comp, and BPT-SF, respectively. The BPT-SF show a trend with color in that the bluer BPT-SF exhibit higher values of [NeIII]/[OII]. This provides a separation in color-space between the BPT-AGN and the BPT-SF with high values of [NeIII]/[OII]. This trend with color is likely due to the fact that bluer galaxies are more metal poor (see Fig. 7 in Tremonti *et al.* (2004)) and hence have harder stellar radiation fields (higher [NeIII]/[OII]; Shi *et al.* 2007). On the other hand, few BPT-AGN reside in very blue galaxies. As discussed in detail in Section 3.3 of Yan *et al.* (2011), nearly all BPT-AGN are found in red galaxies or in galaxies with intermediate colors between red and blue.

The dashed line designates

$$^{0.0}(g - z) = -1.2 \times \log([\mathrm{NeIII}]/[\mathrm{OII}]) - 0.4\,, \tag{2.1}$$

our empirical separation maximizing the fraction of BPT-AGN to total population in

https://doi.org/10.1017/S1743921314003822 Published online by Cambridge University Press

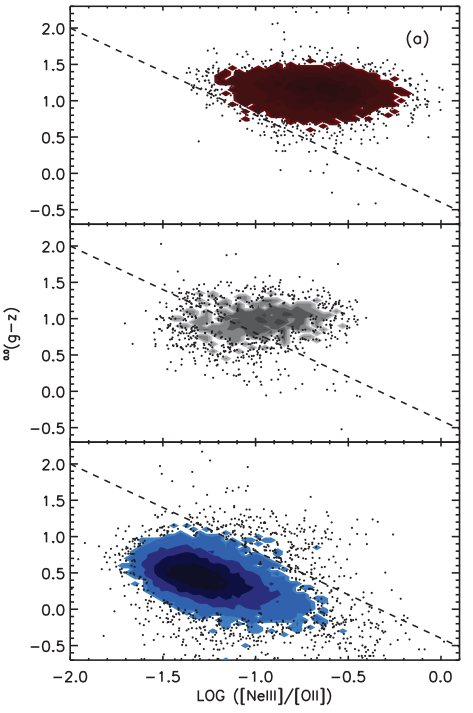

Figure 1. TBT diagram – $^{0.0}(g-z)$ color vs. log([NeIII]/[OII]) – for the SDSS galaxies that have [OIII], Hβ, [NII], Hα, [NeIII], and [OII] fluxes with SNR > 5. The top, middle, and bottom panels show the positions of the BPT-AGN, BPT-comp, and BPT-SF, respectively. The dashed line provides the empirical separation maximizing the fraction of BPT-AGN to total population in the upper-right of the diagram.

the upper-right of the diagram. Hereafter, we refer to the sources in the upper-right (lower-left) of our TBT diagnostic as TBT-AGN (TBT-SF).

We find that 98.7% of the BPT-AGN lie in the TBT-AGN regime and 97.2% of the BPT-SF lie in the TBT-SF regime. Likewise, we find that only 3.5% of the sources in the TBT-AGN regime are BPT-SF and 1% of the sources in the TBT-SF regime are BPT-AGN. The BPT-comp lie on either side of the division, with 68.6% in the TBT-AGN regime. Overall the BPT-comp constitute 5% and 16% of the TBT-SF and TBT-AGN, respectively.

Metallicity Evolution: We have trained our TBT diagnostic on the SDSS galaxies, which have $\langle z \rangle \sim 0.1$. Because our TBT diagnostic can be used with optical spectra out to $z = 1.4$, we examine the impact of metallicity evolution with redshift on our empirical separation between TBT-AGN and TBT-SF. Galaxy metallicities decrease by a factor of ~ 0.3 dex between the local value and the value at $z \sim 2$ (Erb *et al.* 2006). For an $M_{star} = 10^{10} M_{\odot}$ galaxy, this corresponds to a shift from $12 + \log(O/H) = 8.6$ to 8.3 (note that more massive galaxies undergo less metallicity evolution). Using the Shi *et al.* (2007) relation between metallicity and log([NeIII]/[OII]), we find that, in this case, log([NeIII]/[OII]) shifts by only $\sim 20\%$, from -0.89 to -0.72. Applying this 20% increase in the ratio of [NeIII] to [OII] to all SDSS BPT-SF, we find that an additional 5% move to the TBT-AGN regime. This corresponds to an increase of only 5.5% in the number of TBT-AGN that are BPT-SF. Similarly, there is only a 1.8% increase in the number of TBT-AGN that are BPT-comp.

https://doi.org/10.1017/S1743921314003822 Published online by Cambridge University Press

Color Evolution: We also considered the impact of color evolution on our TBT diagnostic. At higher redshifts, galaxies are bluer as a result of higher specific star formation rates. Purely passive evolution models with an instantaneous burst predict a $\Delta^{0.0}(g-z) \sim 0.24$ between $z = 0$ and 1.4, for a formation redshift of 5. Applying this color evolution to all SDSS BPT-SF, the impact is in our favor. The BPT-SF move down the y-axis in our TBT diagnostic to lie even further below our empirical separation, in the TBT-SF regime. Applying this color evolution to all SDSS BPT-AGN, we find that an additional 3.6% move to the TBT-SF regime. This corresponds to an increase of 2.7% in the number of TBT-SF that are BPT-AGN. Similarly, there is only a 2.9% increase in the number of TBT-SF that are BPT-comp.

X-ray Selected AGN: In Trouille *et al.* (2010) we found that 52% of the X-ray selected non-BLAGNs in our OPTX sample lie in the BPT-AGN regime of the BPT diagram and 20% are misidentified as BPT-SF, i.e., as pure star-forming galaxies. Increased extinction does not account for these. Instead, in Trouille *et al.* (2010) we note that these misidentified sources have lower $L_{[\mathrm{OIII}]}/L_X$ ratios than those that lie in the BPT-AGN regime. We postulate that the low forbidden emission line strengths in the misidentified sources are a result of the complexity of the structure of the narrow-line region, which causes ionizing photons from the central engine to not be absorbed.

The misidentification of X-ray selected AGNs as star-forming galaxies is a potential issue for all optical emission-line diagnostic diagrams, including our TBT diagram. However, we find that 97% (100/103) of our OPTX X-ray selected AGNs lie in the TBT-AGN regime. Thus, the TBT diagnostic does a much better job of correctly identifying X-ray selected AGNs than the BPT diagnostic, misidentifying only 3% as TBT-SF compared to the BPT diagnostic's misidentification of 20% as BPT-SF.

References

Alexander, Bauer, Brandt, Schneider, Hornschemeier, Vignali, Barger, Broos, Cowie, Garmire, Townsley, Bautz, Chartas, & Sargent 2003, *AJ*, 126, 539

Baldwin, J. A., Phillips, M. M., & Terlevich, R. 1981, *PASP*, 93, 5

Erb, D. K., Shapley, A. E., Pettini, M., Steidel, C. C., Reddy, N. A., & Adelberger, K. L. 2006, *ApJ*, 644, 813

Juneau, S., Dickinson, M., Alexander, D. M., & Salim, S. 2011, *ApJ*, 736, 104

Kauffmann, Heckman, Tremonti, Brinchmann, Charlot, White, Ridgway, Brinkmann, Fukugita, Hall, Ivezić, Richards, & Schneider, *MNRAS*, 346, 1055

Kewley, L. J., Dopita, M. A., Sutherland, R., Heisler, C. A., & Trevena, J. 2001, *ApJ*, 556, 121

Lamareille, F. 2010, *AAP*, 509, 53

Shi, F., Zhao, G., & Liang, Y. C. 2007, *AAP*, 475, 409

Stasińska, G., Cid Fernandes, R., Mateus, A., Sodré, L., & Asari, N. V. 2006, *MNRAS*, 371, 972

Tremonti, Heckman, Kauffmann, Brinchmann, Charlot, White, Seibert, Peng, Schlegel, Uomoto, Fukugita, & Brinkmann, 2004, *ApJ*, 613, 898

Trouille, L., & Barger, A. J. 2010 *ApJ*, 722, 212

Trouille, L., Barger, A. J., Cowie, L. L., Yang, Y., & Mushotzky, R. F. 2008, *ApJS*, 179, 1

Trouille, Barger, Cowie, Yang, & Mushotzky 2009, *ApJ*, 703, 2160

Trouille, L. and Barger, A. J., & Tremonti, C. 2011, *ApJ*, 742, 46

Wilkes, Kilgard, Kim, Kim, Polletta, Lonsdale, Smith, Surace, Owen, Franceschini, Siana, & Shupe 2009, *ApJS*, 185, 433

Yan, Ho, Newman, Coil, Willmer, Laird, Georgakakis, Aird, Barmby, Bundy, Cooper, Davis, Faber, Fang, Griffith, Koekemoer, Koo, Nandra, Park, Sarajedini, Weiner, & Willner 2011, *ApJ*, 728, 38

Yang, Y., Mushotzky, R. F., Steffen, A. T., Barger, A. J., & Cowie, L. L. 2004, *AJ*, 128, 1501

https://doi.org/10.1017/S1743921314003822 Published online by Cambridge University Press